Video imaging of biomolecular processes by high-speed AFM

doi: 10.1109/MEMSYS.2011.5734361

VIDEO IMAGING OF BIOMOLECULAR PROCESSSES BY HIGH-SPEED AFM

T. Ando[1,2]
[1]Department of Physics and [2]Bio-AFM Frontier Research Center,
Kanazawa University, Kanazawa, JAPAN

ABSTRACT

The imaging rate of conventional atomic force microscopy (AFM) is too low to capture the dynamic behavior of biomolecules. To overcome this problem, we have been developing various devices and techniques, including small cantilevers and high-speed scanners. The feedback bandwidth in the tapping-mode now exceeds 100 kHz and hence the maximum possible imaging rate reaches 25 frames per sec (fps). Importantly the tip-force exerting onto the sample is dramatically reduced. Thus, it is now possible to take video images of dynamically moving protein molecules in action without disturbing their function, including walking myosin V molecules along actin tracks.

INTRODUCTION

AFM [1] has been widely used to observe nanometer-scale objects under various environments. In AFM, a micro cantilever with a sharp tip at the free end plays an essential role in the imaging mechanism. The cantilever tip interacts with a tiny portion of the sample surface. The cantilever acts like an 'objective lens' in optical microscopy and the nano-scale tip-sample interaction is transmitted to the micro-scale cantilever. The interaction portion is varied over an imaging area of the sample by the xy-scanning of the sample stage or the cantilever tip while the tip-sample interaction force is maintained constant by the feedback-controlled z-scanning. A series of these operations over many surface portions requires a considerable time and therefore the imaging rate is quite low. In biological applications of AFM, this low imaging rate means that we can only observe stationary samples or considerably slow biological processes.

Proteins are dynamic in nature and hence it is essential to observe their dynamic behavior to understand how they function. Single-molecule biology was thus founded more than 20 years ago [2-4]. The main technique used therein is single-molecule fluorescence microscopy. However, protein molecules themselves are invisible in the observations even using super-resolution fluorescence microscopy [5-7]. The structure of proteins has been studied by x-ray crystallo-graphy, electron microscopy, NMR, or AFM but the obtainable structures are essentially static. The concomitant observation of structure and dynamics is infeasible, which has been preventing us from comprehensive understanding how proteins function.

To overcome this long-standing problem and make it possible to record the structure and dynamics of functioning protein molecules simultaneously, We have been developing high-speed AFM [8-20]. The recent significant improvement in its performance has been demonstrated in several bio-imaging studies [21-28]. Here, I present the theoretical basis for the feedback bandwidth and imaging rate, instrumentation, and some imaging studies of proteins in acion.

FEEDBACK BANDWIDTH AND IMAGING RATE

When a sample is scanned over an area of $W \times W$ with scan velocity V_s in the x-direction and N scan lines in the y-direction, the image acquisition time T is given by $T = 2WN/V_s$. Supposing that the sample surface is characterized with a single spatial frequency $1/\lambda$, then the feedback z-scan is executed with frequency $f = V_s/\lambda$ to trace the sample surface. The feedback bandwidth f_B of the microscope should be equal to or higher than f, and thus, we obtain the relationship $T \geq 2WN/(\lambda f_B)$ [20].

The feedback bandwidth is usually defined by a feedback frequency at which a closed-loop phase delay of $\pi/4$ occurs in tracing the sample surface. The phase delay in the closed loop (φ_{closed}) is approximately twice that in the open loop (φ_{open}), provided the feedback gain is maintained at ~1 [20]. The phase delay is caused by the limited response speed of devices contained in the feedback loop and by the time delay due to a below-mentioned 'parachuting' effect. By denoting the total time delay by $\Delta\tau_{total}$, φ_{open} is given by $\varphi_{open} = 2\pi f\Delta\tau_{total}$. The phase delay can be compensated by a factor of α (2-3) using the (P + D) operation of the proportional-integral-derivative (PID) feedback controller. f_B is thus given by $f_B = \alpha/(16\Delta\tau_{total})$ [20]. Hence, the highest possible imaging rate (V_{max}) is give by $V_{max} = \alpha\lambda/(32WN\Delta\tau_{total})$, when the sample fragility is not taken into account. To materialize, for example, an imaging rate of 25 fps for $\alpha = 2.5$, $\lambda = 10$ nm, $W = 200$ nm, and $N = 100$, we have to achieve $f_B > 100$ kHz and thus $\Delta\tau_{total} < 1.6$ μs.

SMALL CANTILEVERS

The response time of a cantilever τ_c is expressed by $\tau_c = Q_c/(\pi f_c)$, where Q_c and f_c are the quality factor and resonant frequency of a cantilever, respectively. To shorten the response time, we need a high f_c and a small Q_c. Not only the response time but also the time required to measure the cantilever oscillation amplitude is one of factors causing a feedback delay. The minimum time for measuring the amplitude τ_d is given by $1/(2f_c)$ Thus, the cantilever's resonant frequency is the most important element in increasing the feedback bandwidth. The resonant frequency f_c and the spring constant k_c of a rectangular cantilever with length L, width w, and thickness d are respectively given by

$$f_c = 0.56\frac{d}{L^2}\sqrt{\frac{E}{12\rho}} \qquad (1)$$

and

$$k_c = \frac{wd^3}{4L^3}E\,, \qquad (2)$$

where E and ρ are the Young's modulus and density of the material used, respectively. For given k_c, w, and material, f_c increases in inverse proportion to $(Ld)^{1/2}$. Therefore, we have to fabricate short and thin cantilevers to simultaneously achieve a high resonant frequency and a small spring constant [29].

We developed small cantilevers collaborating with Olympus [8, 30]. The most recent small cantilevers made of Si_3N_4 are ~6 μm long, 2 μm wide, and 90 nm thick (Fig. 1a), resulting in f_c in air 3.5 MHz, f_c in water 1.2 MHz, k_c ~0.2 N/m, and Q_c in water 2-3 [20]. Therefore, τ_c andτ_d in water are 0.66 μs and 0.42 μs, respectively. Somewhat larger cantilevers (BL-AC10DS-A2, Olympus: f_c in air 1.5 MHz, f_c in water 600 kHz, k_c ~0.1 N/m) are already commercially available (Atomic Force F&E GmbH).

In addition to the advantage in achieving a high imaging rate, small cantilevers have other advantages. The total thermal noise only depends on the spring constant and the temperature. Therefore, a cantilever with a higher resonant frequency has a lower noise density. In addition, shorter cantilevers have higher optical beam deflection (OBD) detection sensitivity, because the sensitivity follows $\Delta\theta/\Delta z = 3/(2L)$, where Δz is the displacement and $\Delta\theta$ is the change in the angle of a cantilever free-end. A high resonant frequency and a small spring constant result in a large ratio (f_c/k_c), which grants the cantilever high sensitivity to the gradient (k) of the force exerted between the tip and the sample, because the force gradient shifts the cantilever resonant frequency by approximately $-0.5kf_c/k_c$. Therefore, small cantilevers with large values of f_c/k_c are useful for phase-contrast imaging and frequency-modulation AFM.

CANTILEVER TIP

The tip apex radius of the small cantilevers developed by Olympus is ~17 nm, which is not sufficiently small for the high-resolution imaging of biological samples. We attach a sharp tip on the original tip by electron-beam deposition (EBD) in phenol gas [20]. A piece of phenol crystal (sublimate) is placed in a small container with small holes (~0.1 mm diameter) in the lid. The container is placed in a scanning electron microscope (SEM) chamber under a low-vacuum condition, and cantilevers are placed immediately above the holes. A spot-mode electron beam is irradiated onto the cantilever tip, which produces a needle on the original tip at a growth rate of ~1 μm/min. The newly formed tip has an apex radius of ~25 nm and is sharpened by plasma etching in argon or oxygen gas (Fig. 1b), which decreases an apex radius to ~4 nm in the best case. However, it is still an ultimate goal that cantilevers with a sharp tip are fabricated in a single process since piece-by-piece attachment of an EBD tip is time consuming and increases the production cost.

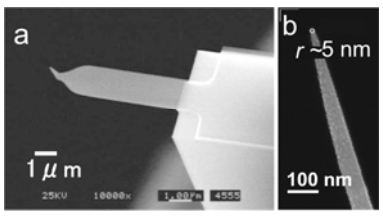

Fig. 1. SEM images of small cantilever (a) and EBD tip (b).

OTHER DEVICES

Piezoactuator-based Scanner

The response time of the z-scanner is expressed by $\tau_s = Q_s/(\pi f_s)$, where Q_s and f_s are the quality factor and resonant frequency of the z-scanner, respectively. The resonant frequency is almost determined by the z-piezo used and by how hold it. As f_s and the maximum possible displacement are inversely related, f_s is almost determined by how much displacement is required. We use a piezoactuator (3×3×3 mm^3) with a maximum displacement of 2 μm and f_s ~ 400 kHz and hold it at the four rims parallel to the displacement direction [19]. This holding can keep f_s unchanged, although the usable maximum displacement is reduced to the half of the original value.

To damp unwanted vibrations of the z-scanner and thereby reduce τ_s, we developed a feedback Q-control method that uses a mock z-scanner (an LRC circuit) which is characterized by a transfer function similar to that of the z-scanner [10]. The output of the mock z-scanner responds to the piezo driving signal in a way very similar to the displacement of the z-piezo and hence can be used to generate a damping signal which is added to the driving signal (Fig. 2). Using this damping method, we have achieved τ_s ~ 0.64μs.

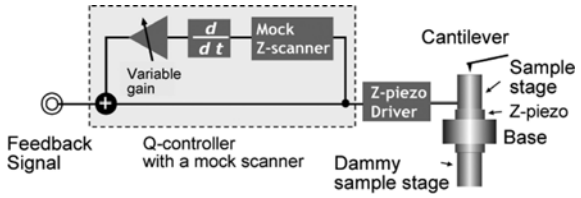

Fig. 2. Feedback Q-control system for damping unwanted vibrations of the z-scanner.

Some researchers have been attempting to construct MEMS-based high-speed scanners. However, MEMS devices do not produce a large force and are apt to be influenced by the mass of objects (such as a sample stage) to be attached to. Thus far, this approach has not been successful. It is still an ultimate goal to create an actuator which can produce a large force and possesses a high extension coefficient.

Parachuting and Dynamic PID controller

It is difficult to make high-speed imaging compatible with low invasive imaging. In order for the oscillating cantilever tip to tap the sample surface with a small force, the

set point (cantilever oscillation amplitude to be maintained during imaging) has to be set very close to the free oscillation amplitude. Under this condition, however, the tip often completely detaches from the sample surface at steep downhill regions of the sample (parachuting). Once detached, the error signal is saturated at a small level, and hence, it takes a long time for the detached tip to re-land on the surface, which significantly reduces the feedback bandwidth.

We solved this problem by devising a PID controller with a capability to automatically change the PID's gain parameters depending on the cantilever oscillation amplitude [14]. When the amplitude exceeds the amplitude set point, the gains are increased. The oscillation amplitude thereby quickly returns towards the set point before the error signal is saturated. Consequently, the feedback bandwidth becomes independent of the set point as long as the set point is smaller than ~0.95 (Fig. 3).

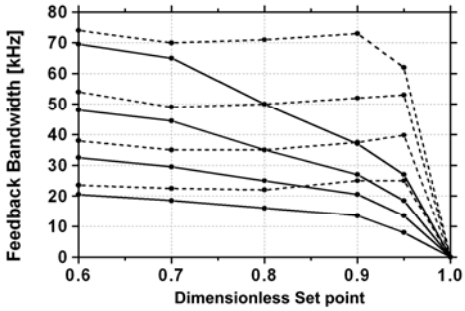

Fig. 3. Feedback bandwidth vs. set point. Solid line, conventional PID control; broken line, dynamic PID control. Feedback bandwidth is also affected by the ratio of the cantilever free oscillation amplitude to the maximum sample height. The two sets of lines are aligned from the top to the bottom according to the ratio 5, 2, 1, and 0.5

BIOIMAGING

In addition to the above mentioned techniques and devices, several techniques were further developed, including a technique to compensate for drift in the cantilever excitation efficiency [14] and an OBD detector with high bandwidth. As a result, the feedback bandwidth reached ~110 kHz and the maximum possible imaging rate reached ~25 fps for the scan range 240×240 nm^2, 100 scan lines, and the spatial frequency of the sample surface corrugation 1/10 nm^{-1}. The peak tapping force exerting from the oscillating cantilever tip to the sample is about 30 pN. It sounds large compared to the force generated by motor proteins (~ a few pN). However, the mechanical quantity that affects the sample is not the force itself but impulse; *i.e.*, force × force acting time. The resonant frequency of our small cantilevers is ~1.2 MHz and hence the force acting time is less than 100 ns. So, the magnitude of impulse is very small. Hereinafter, we show results of high-speed AFM imaging of proteins.

Walking Myosin V

Myosin V (M5) is similar to muscle myosins but has unique properties (reviewed in [31]). This two-headed motor protein acts as a cargo transporter in cells. Each head consists of an N-terminal motor domain and a long neck, which is followed by a coiled-coil tail and terminated with a cargo binding domain. M5 moves processively along actin tracks taking ~36 nm steps, in a hand-over-hand manner (*i.e.*, two heads alternate between leading and trailing positions on actin, just like 'walking'. These features have been studied by fluorescence microscopy, and therefore, revealing the details of walking behavior and chemo-mechanical coupling is still a challenge.

To observe walking M5 molecules, M5 has to be kept free from the substrate surface. We used a surface of mica-supported bilayer of electrically neutral phospholipids since the surface is resistant to non-specific binding of proteins. However, a small amount of a positively charged lipid was added to facilitate the weak sideways adsorption of tail-truncated myosin V (M5-HMM) onto the surface. Partially biotinylated actin filaments were immobilized on the surface using biotin-lipid and streptavidin. Fig. 4 shows images of M5-HMM moving processively with 36-nm steps. A processive run almost always continued to the full extent of each imaging range used (4–16 steps). The observed translocation velocity was 70% of previously reported values. This is due to the sample-surface interaction, not due to the tip-sample interaction.

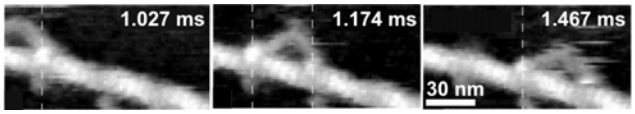

Fig. 4. Successive AFM images showing processive movement of M5-HMM in 1 μM ATP.

As observed above, the 36-nm advance was completed within one frame (146.7 ms); therefore, the molecular process occurring during a step could not be resolved. However, additional streptavidin molecules placed on the substrate surface as moderate obstacles to the advance allowed the visualization of this process (Fig. 5a, b). After trailing head detachment, the nearly straight leading neck swung from the backward orientation to the forward orientation, confirming the swinging lever-arm motion initially proposed for muscle myosin [32]. The detached trailing head rotationally diffused around the advancing neck–neck junction and then bound to a forward site on the actin filament, completing one step. Thus, the hand-over-hand movement, including the intermediate process, was directly visualized at high resolution. The captured images show that the forward movement is driven not by bending but by rotation of the leading head. The rotation seems to occur spontaneously after trailing head detachment, suggesting that intramolecular tension driving the leading head swing exists in the two-headed bound molecules.

These molecular movies provide not only corroborative 'visual evidence' for previously speculated or demonstrated molecular behaviors but also reveal previously unknown behaviors including 'foot stomp'-like behavior in which

either of the heads briefly detaches from actin and then rebinds. The foot stomp indicates that force generation by the leading head occurs without transitioning in the chemical state (see the original paper for details).

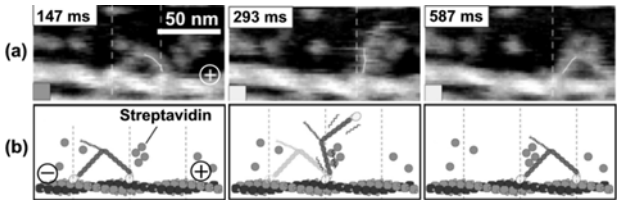

Fig. 5. (a) Successive AFM images showing hand-over-hand movement in 1 μM ATP. (b) Schematic explaing the images in (a). The plus and minus signes indicate the polarity of actin.

Photo-activated Bacteriorhodopsin

The membrane protein, bacteriorhodopsin (bR), found in the purple membrane (PM) of *Halobacterium salinarum*, functions as a light-driven proton pump transferring protons across the membrane from the cytoplasmic side to the extracellular side (reviewed in [33, 34]). bR is comprised of seven transmembrane α-helices (named A-G) surrounding the retinal chromophore covalently bound to Lys216 via a protonated Schiff base. Upon absorption of light, photo-isomerization from all-*trans* to 13-*cis* conformation of the retinal takes place, followed by the primary proton transfer from the Schiff base to Asp85 that triggers a cascade of changes in the bR structure. A series of intermediates designated J, K, L, M, N, and O are defined by spectroscopy and M (M_{410}) is the only intermediate containing a deprotonated Schiff base. While numerous structural studies of bR in the unphotolyzed or frozen activated states have been reported, dynamic structural changes of bR upon light illumination have been poorly understood because of the lack of techniques.

We first attempted to visualize the dynamic structural changes in the wild type bR but could not do so even at 100 fps as the photocycle is completed in 10 ms. Therefore, we used D96N bR mutant which has a long photocycle time (~10 s) but retains the ability of proton pumping. Fig. 6 shows high-speed AFM images of the cytoplasmic surface of D96N under dark and illuminated conditions (532 nm green light, 0.5 μW) [25]. Upon light illumination, the center of mass of each bR molecule moved outward by 0.7 nm and rotated counterclockwise around the trimer center by 7.4° (Fig. 6a-d). After the light is turned off, bR returns to the unphotolyzed state in a few seconds. The observed change is much larger than that suggested in previous studies. The overall position of each bR molecule does not change because of indiscernible alterations at the extracellular surface. Comparison of the AFM images of the cytoplasmic side with an atomic model of the unphotolyzed bR structure indicates that the outward movement of the center of mass is caused by the outward displacement of the E-F loop (Fig. 6e, f).

As a result of the outward displacement of the E-F loop, three nearest-neighbor bR monomers, each belonging to a different adjacent trimer, transiently assemble (Fig. 6b, d). The triad of nearest-neighbor monomers is designated "trefoil". This transient assembly in a trefoil alters the decay kinetics of the activated state. When only one bR monomer in a trefoil was excited under weak illumination, it decayed with a time constant of 7.3 s. When two or three bR monomers in a trefoil were excited under strong illumination, they decayed with a short or long time constant (2 s or 13 s). The decay time of each monomer depends on the order of its activation. The monomer that is activated latest among the activated monomers in the trefoil decays with the short time constant. On the other hand, the decay kinetics of the early activated monomers does not follow a single exponential, and the monomers decay with the long time constant on average. Thus, the monomer-monomer interaction in the trefoil engenders both positive and negative cooperative effects in the decay kinetics as the initial bR recovers. Consequently, the average rate of proton pumping by the activated bR is conserved independently of the light intensity. This is perhaps the reason why bR naturally exists in the form of a crystal in PM.

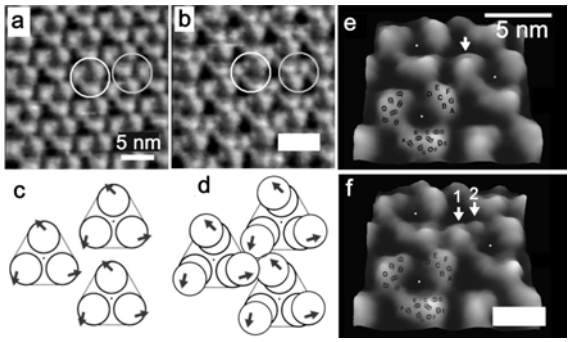

Fig. 6. AFM images showing structural changes in bR by photo-activation. (a, b) Cytoplasmic surface of bR under dark (a) and illuminated (b) conditions. White circles, trimer; gray circles, trefoil. The white bar in (b) indicates light illumination. (c, d) Schematic of the images in (a) and (b), respectively. The arrows indicate the directions of bR movement. (e, f) High- resolution images under dark (e) and illuminated (f) conditions. The single protrusion (arrow in e) is split into two (arrows in f).

DISCUSSION

MESM and High-speed AFM

Historically, attempts to increase the AFM imaging rate were initiated in 1991 by Quate and colleagues [35]. They aimed at fast inspection or lithography of a wide range of surfaces of hard materials, rather than at observing biomolecular processes. Images (a few μm scan range) of a metal-semiconductor transistor were taken at 3.3 fps in the constant-height mode (no feedback scan in the z-direction) [35]. This study proceeded towards the development of cantilevers or cantilever arrays with integrated sensors and/or actuators [36, 37] but fabricating these cantilevers was only possible in relatively large dimensions, resulting in low resonant frequencies and large spring constants. Insulation coating of the integrated cantilevers for the use in liquids further lowered the resonant frequency.

However, it is still an ultimate goal to fabricate small cantilevers with self-sensing and self-actuation capabilities in water as well as a high resonant frequency and a small spring constant. Such cantilevers not only simplify the structure of a high-speed AFM apparatus but also have a potential to further increase the imaging rate. At present, in our high-speed AFM, the imaging rate is mainly limited by the resonant frequencies of small cantilevers and z-piezo-actuators. The reason for the limited resonant frequency of small cantilevers is that a cantilever has to have a certain lowest limit in the dimensions for the compatibility with the OBD detection. Self-sensing cantilevers may be able to overcome the dimension limit.

Conventional piezoactuators extend only ~0.1% of their length. This means that we have to use a piezoactuater with a certain length that meets a maximum displacement required for the z-scanner, which determines the available highest resonant frequency as a matter of course. It is a challenge to discover new piezo materials with much higher extension coefficients. Alternatively, it may be possible to fabricate new actuators by MEMS techniques.

Future Prospects of High-speed Bio-AFM

Although high-speed AFM capable of imaging dynamic biomolecular processes has been at last materialized, a variety of high-speed AFM apparatuses are still needed for biological research; high-speed recognition AFM, high-speed non-contact AFM, high-speed diaphano-AFM, and ultra high-speed non-contact AFM. For example, we desire to observe dynamic biomolecular processes that occur on the live cell surfaces and dynamic processes of organelles that occur in the interior of live cells.

Cell membranes are extremely soft, particularly those of eukaryotes. Therefore, when a cantilever tip makes contact with a cell membrane, the cell is largely deformed before a detectable change in the deflection or oscillation amplitude of the cantilever appears. Moreover, cell membranes are highly fluidic and hence membrane proteins that are not assembled or not anchored to cytoskeletons in the cytoplasmic side are highly mobile. Therefore, we need ultra high-speed non-contact AFM.

Recently, scanning near-field ultrasound holography (SNFUH) has been developed for high-resolution sub-surface imaging [38]. A high-frequency acoustic wave (frequency f_1) is launched from under the sample stage, and this wave then propagates through the sample. Materials embedded in the sample with different elastic modulus/density rations modulate the phase and amplitude of the propagating acoustic wave. When the resonant frequency of the cantilever f_c is comparable with f_1, the modulated acoustic wave can be directly detected by the cantilever. When $f_1 >> f_c$, another acoustic wave with a frequency f_2 ($|f_1 - f_2| \sim f_c$) is launched from the cantilever base. The non-linear tip-sample interaction generates an acoustic wave with a frequency $|f_1 - f_2|$, and therefore, the cantilever is excited by the generated acoustic wave. SNFUH has a potential to image intracellular structures. At present, however, this method can only image artificial solid particles introduced in cells because of limited contrast for intracellular organelles [39]. To gain high contrast for intrinsic cellular materials, we need very high frequency acoustic wave. To observe dynamic events occurring in the interior of cells, we additionally need a fast and high-sensitive phase detector. Again, MEMS techniques will be able to contribute to the materialization of high-speed diaphano-AFM by fabricating very high frequency acoustic devices.

REFERENCES

[1] G. Binnig, C.F. Quate, Ch. Gerber, "Atomic force microscope", *Phys. Rev. Lett*., vol. 56, pp. 930-933, 1986.

[2] Y. Sako, T. Yanagida, "Review: single-molecule visualization in cell biology", *Nature Rev. Mol. Cell Biol.* vol. 4,pp. SS1–SS5, 2003.

[3] M. I. Wallace, J. E. Molloy, D. R. Trentham, "Minireview: combined single-molecule force and fluorescence measurements for biology", *J. Biol*. vol. 2, pp. 4-8, 2003.

[4] P. V. Cornish, T. Ha, "A survey of single-molecule techniques in chemical biology", *ACS Chem. Biol*. vol. 2, pp. 53-61, 2007.

[5] E. Betzig, G. H. Patterson, R. Sougrat, O. W. Lindwasser, S. Olenych, J. S. Bonifacino, M. W. Davidson, J. Lippincott-Schwartz, H. F. Hess, "Imaging intracellular fluorescent proteins at nanometer resolution", *Science*, vol. 313, pp. 1642-1645, 2006.

[6] M. Bates, B. Huang, G. T. Dempsey, X. Zhuang, "Multicolor super-resolution imaging with photo-switchable fluorescent probes", *Science*, vol. 317, pp. 1749-1753, 2007.

[7] K. I. Willig, S. O. Rizzoli, V. Westphal, R. Jahn, S. W. Hell, "STED microscopy reveals that synaptotagmin remains clustered after synaptic vesicle exocytosis", *Nature*, vol. 440, pp. 935-939, 2006.

[8] T. Ando, N. Kodera, E. Takai, D. Maruyama, K. Saito, A. Toda, "A high-speed atomic force microscope for studying biological macromolecules", *Proc. Natl. Acad. Sci. USA*, vol. 98, pp. 12468-12472, 2001.

[9] T. Ando, N. Kodera, D. Maruyama, E. Takai, K. Saito, A. Toda, "A high-speed atomic force microscope for studying biological macromolecules in action", *Jpn. J. Appl. Phys.*, vol. 41, pp. 4851-4856, 2002.

[10] N. Kodera, H. Yamashita, T. Ando, "Active damping of the scanner for high-speed atomic force microscopy", *Rev. Sci. Instrum.*, vol. 76, 053708 (5 pp), 2005.

[11] T. Ando, T. Uchihashi, N. Kodera, A. Miyagi, R. Nakakita, H. Yamashita, K. Matada, "High-speed AFM for studying the dynamic behavior of protein molecules at work", *Surf. Sci. Nanotechnol.*, vol. 3, pp. 384-392, 2005.

[12] T. Uchihashi, N. Kodera, H. Itoh, H. Yamashita, T. Ando, "Feed-forward control for high-speed AFM imaging of biomolecules", *Jpn. J. Appl. Phys.*, vol. 45, pp. 1904-1908, 2006.

[13] T. Ando, T. Uchihashi, N. Kodera, A. Miyagi, R. Nakakita, H. Yamashita, M. Sakashita, "High-speed atomic force microscopy for studying the dynamic behavior of protein molecules at work", *Jpn. J. Appl. Phys*., vol. 45, pp. 1897-1903, 2006.

[14] N. Kodera, M. Sakashita, T. Ando, "Dynamic proportional-integral-differential controller for high-speed atomic force microscopy", *Rev. Sci. Instrum.*, vol. 77, 083704 (7 pp), 2006.

[15] T. Uchihashi, H. Yamashita, T. Ando, "Fast phase imaging in liquids using a rapid scan atomic force microscope", *Appl. Phys. Lett*., vol. 89**,** 213112 (3 pp), 2006.

[16] H. Yamashita, T. Uchihashi, N. Kodera, A. Miyagi, D. Yamamoto, T. Ando, "Tip-sample distance control using photo-thermal actuation of a small cantilever for high-speed atomic force microscopy", *Rev. Sci. Instrum.*, vol. 78, 083702 (5 pp), 2007.

[17] T. Ando, T. Uchihashi, N. Kodera, D. Yamamoto, M. Taniguchi, A. Miyagi, H. Yamashita, "Review: High-speed atomic force microscopy for observing dynamic biomolecular processes", *J. Mol. Recognit.*, vol. 20, pp. 448-458, 2007.

[18] T. Ando, T. Uchihashi, N. Kodera, D. Yamamoto, M. Taniguchi, A. Miyagi, H. Yamashita, "Invited Review: High-speed AFM and nano-visualization of biomolecular processes", *Pflügers Archiv -Eur. J. Physiol.*, vol. 456, pp. 211-225, 2008.

[19] T. Fukuma, Y. Okazaki, N. Kodera, T. Uchihashi, T. Ando, "High resonance frequency force microscope scanner using inertia balance support", *Appl. Phys. Lett.*, vol. 92, 243119 (3 pp), 2008.

[20] T. Ando, T. Uchihashi, T. Fukuma, "High-speed atomic force microscopy for nano-visualization of dynamic biomolecular processes", *Prog. Surf. Sci.*, vol. 83, pp. 337-437, 2008.

[21] A. Miyagi, Y. Tsunaka, T. Uchihashi, K. Mayanagi, S. Hirose, K. Morikawa, T. Ando, "Visualization of intrinsically disordered regions of proteins by high-speed atomic force microscopy", *Chem. Phys. Chem.*, vol. 9, pp. 1859-1866, 2008.

[22] D. Yamamoto, T. Uchihashi, N. Kodera, T. Ando, "Anisotropic diffusion of point defects in two-dimensional crystal of streptavidin observed by high-speed atomic force microscopy", *Nanotechnol.*, vol. 19, 384009 (9 pp), (2008).

[23] H. Yamashita, K. Voïtchovsky, T. Uchihashi, S. Antoranz Contera, J. F. Ryan, T. Ando, "Dynamics of bacteriorhodopsin 2D crystal observed by high-speed atomic force microscopy", *J. Struct. Biol.*, vol. 167, pp. 153-158, 2009.

[24] D. Yamamoto, N. Nagura, S. Omote, M. Taniguchi, and T. Ando, "Streptavidin 2D crystal substrates for visualizing biomolecular processes by atomic force microscopy", *Biophys. J.*, vol. 97, pp. 2358–2367, 2009.

[25] M. Shibata, H. Yamashita, T. Uchihashi, H. Kandori, T. Ando, "High-speed atomic force microscopy shows dynamic molecular processes in photo-activated bacteriorhodopsin", *Nature Nanotechnol*., vol. 5, pp. 208-212, 2010.

[26] M.-C. Giocondi, D. Yamamoto, E. Lesniewska, P.-E. Milhiet, T. Ando, C. Le Grimellec, "Surface topography of membrane domains", *Biochim. Biophys. Acta.-Biomembranes*, vol. 1978, pp. 703-718, 2010.

[27] P.-E. Milhiet, D. Yamamoto, O. Berthoumieu, P. Dosset, C. Le Grimellec, J.-M. Verdier, S. Marchal, T. Ando, "Deciphering the structure, growth and assembly of amyloid-like fibrils using high-speed atomic force microscopy", *PLos One*, vol. 5, e13240 (8 pp), 2010.

[28] Noriyuki Kodera, Daisuke Yamamoto, Ryoki Ishikawa, and Toshio Ando, "Video imaging of walking myosin V by high-speed atomic force microscopy", *Nature*, vol. 468, pp. 72-76, 2010.

[29] D. A. Walters, J. P. Cleveland, N. H. Thomson, P. K. Hansma, M. A. Wendman, G. Gurley, V. Elings, "Short cantilevers for atomic force microscopy", *Rev. Sci. Instrum*., vol. 67, pp. 3583-3590, 1996.

[30] M. Kitazawa, K. Shiotani, A. Toda, "Batch fabrication of sharpened silicon nitride tips", *Jpn. J. Appl. Phys*. vol. 42, pp. 4844-4847, 2003.

[31] J. R. Sellers, L. S. Weisman, in *Myosins: A superfamily of molecular motors, proteins and cell regulation* (ed. L. Coluccio), pp. 289-324, Springer, 2008.

[32] H. E. Huxley, "The mechanism of muscular contraction", *Science*, vol. 164, pp. 1356–1366, 1969.

[33] U. Haupts, J. Tittor, D. Oesterhelt, "Closing in on bacteriorhodopsin: progress in understanding the molecule", *Annu. Rev. Biophys. Biomol. Struct.*, vol. 28, pp. 367-399, 1999.

[34] J. K. Lanyi, "Bacteriorhodopsin", *Annu. Rev. Physiol.*, vol. 66, pp. 665-688, 2004.

[35] R. C. Barrett, C. F. Quate, "High-speed, large-scale imaging with the atomic force microscope", *J. Vac. Sci. Technol.*, vol. B9, pp. 302-306, 1991.

[36] S. C. Minne, S. R. Manalis, C. F. Quate, "Parallel atomic force microscopy using cantilevers with integrated piezoresistive sensors and integrated piezoelectric actuators", *Appl. Phys. Lett*., vol. 67, pp. 3918-3920, 1995.

[37] S. R. Manalis, S. C. Minne, C. F. Quate, "Atomic force microscopy for high speed imaging using cantilevers with an integrated actuator and sensor", *Appl. Phys. Lett*., vol. 68, pp. 871-873 (1996).

[38] G. S. Shekhawat, V. P. Dravid, "Nanoscale imaging of buried structures via scanning near-field ultrasound holography", *Science*, vol. 310, pp. 89-92, 2005.

[39] L. Tetard, A. Passian, K. T. Venmar, R. M. Lynch, B. H. Voy, G. Shekhawat, V. P. Dravid, T. Thundat, "Imaging nanoparticles in cells by nanomechanical holography", *Naure Nanotechnol.*, vol. 3, pp. 501-505, 2008.